iScience

CellPress
OPEN ACCESS

Article

Proteomic and metabolomic profiling of plasma predicts immune-related adverse events in older patients with advanced non-small cell lung cancer

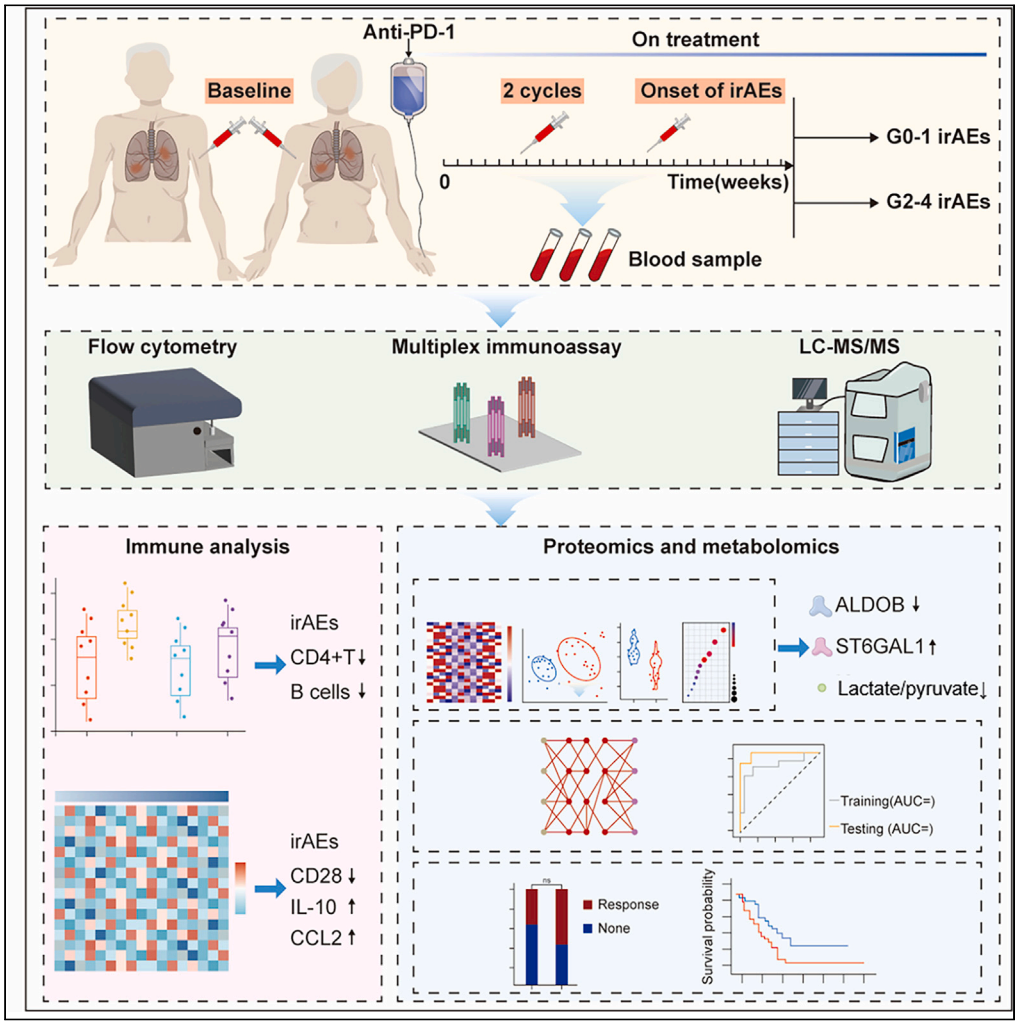

Jiayi Gao, Ping Zhang, Xin Nie, ..., Xue Wang, Junling Ma, Lin Li

lilin_51@hotmail.com

Highlights

Expression of ALDOB, lactate/pyruvate ratio, and ST6GAL1 were associated with irAEs

Plasma metabolites changes predict the occurrence of irAEs

Lower ALDOB expression and a lower lactate/pyruvate ratio indicate a good prognosis

Gao et al., iScience 27, 109946
June 21, 2024
https://doi.org/10.1016/j.isci.2024.109946

iScience

CellPress
OPEN ACCESS

Article

Proteomic and metabolomic profiling of plasma predicts immune-related adverse events in older patients with advanced non-small cell lung cancer

Jiayi Gao,[1,2] Ping Zhang,[1] Xin Nie,[1] Min Tang,[1] Yue Yuan,[1] Liuer He,[1] Xue Wang,[1] Junling Ma,[1] and Lin Li[1,2,3,*]

SUMMARY

The clinical success of immune checkpoint inhibitors is compromised by the fact of immune-related adverse events (irAEs), especially for older patients. To identify predictive biomarkers for older patients with irAEs, we used multiplex immunoassay and flow cytometry and liquid chromatography-tandem mass spectrometry to test immune factors and plasma protein and metabolites levels in non-small cell lung cancer (NSCLC) patients. The results showed that older patients with irAEs displayed lower CD28, $CD4^+$ T cell, and B cell and higher interleukin (IL)-10 and CCL2 levels at baseline. Besides, lower aldolase, fructose-bisphosphate B (ALDOB), higher ST6GAL1, and lower lactate/pyruvate ratio at baseline were found in older patients with irAEs. Based on metabolomic markers, predictive models were developed to distinguish patients with grade 2–4 irAEs from grade 0–1 (Area under curve, AUC = 0.831) and to distinguish patients with grade 3–4 irAEs from grade 2 (AUC = 1). Our results confirmed the predictive value of plasma metabolites for irAEs in older patients with NSCLC.

INTRODUCTION

Immune checkpoint inhibitors (ICIs), such as anti-programmed cell death 1 (PD-1) and anti-programmed cell death ligand 1 (PD-L1), have transformed the management of several types of cancers. The clinical success of ICIs is compromised by a series of immune-related adverse events (irAEs). According to statistics, irAEs comprise over 70 different pathologies affecting nearly every organ system, including the skin, colon, lungs, kidneys, and endocrine systems. The incidence of irAEs was approximately 60% for any grade and 20% for severe grade.[1] Grade ≥ 3 irAEs come with the recommendation of discontinuing all further immunotherapy, and grade 2 irAEs come with the suspension of immunotherapy, both of which ultimately affect their oncologic outcome. As the use of ICIs has become more widespread, significant attention should be paid to the management of severe irAEs.

Lung cancer is regarded as a disease of older adults because nearly two-thirds of patients at initial diagnosis are older than 65 years.[2] Compared with highly toxic chemotherapies, immunotherapy is an excellent alternative option with a survival benefit and low toxicity for older adults.[3,4] However, the emergence of immunosenescence- and senescence-associated secretory phenotypes accompanied by advancing age raises safety concerns for these drugs.[5,6] Previous studies have revealed a higher incidence of irAEs in older patients with non-small cell lung cancer (NSCLC), either as a monotherapy or in combination with chemotherapy.[7–10] In addition, irAEs have a detrimental effect on the quality of life and may lead to treatment interruptions, especially in older patients with impaired functional reserve. Therefore, focusing on irAEs in older patients with lung cancer is necessary to improve their quality of life and prolong their survival.

The exploration of predictive biomarkers to distinguish patients who are more likely to suffer irAEs from overall individuals has great implications. A large number of immune biomarkers, including lymphocytes and cytokines from the peripheral blood, have been identified to predict irAEs. Early studies have shown that the circulating T cell repertoire and clonal expansion of $CD8^+$ T cells are associated with immune response and toxicity.[11,12] Recent reports have demonstrated that activated $CD4^+$ effector memory T cells and the lower level of Breg cell are predictors of development of irAEs.[13,14] Furthermore, interleukin (IL)-10, a polygenic and polypotent cytokine, has been reported to be linked to irAEs.[15,16] However, these data did not show robust correlation and repeatability owing to the limited sample size.

Metabolic programs direct the survival, proliferation, and effector functions of immune cells. Previous studies revealed that dysregulated metabolism of T cells in the tumor microenvironment affects the immune response.[17] Combining metabolic inhibition and anti-PD-1 immunotherapy dramatically improved antitumor effects compared with anti-PD-1 therapy alone.[18] Furthermore, metabolomic profiling of peripheral blood has recently been reported to evaluate immune responses in cancers treated with ICIs.[19–21] However, the role of metabolic regulation in the development of irAEs remains underexplored. Considering the mechanism of irAEs, we hypothesized that metabolomic profiling of plasma at baseline could help predict the occurrence of irAEs.

[1]Department of Oncology, Beijing Hospital, National Center of Gerontology; Institute of Geriatric Medicine, Chinese Academy of Medical Sciences, Beijing 100730, P.R. China
[2]Graduate School Peking Union Medical College, Beijing 100730, China
[3]Lead contact
*Correspondence: lilin_51@hotmail.com
https://doi.org/10.1016/j.isci.2024.109946

Table 1. Immune-related adverse events in all patients (*n* = 46)

Immune-related adverse events	Total	Grade 1	Grade 2	Grade 3–4
Interstitial pneumonia	15	5	6	4
Dermatological toxicity	12	5	4	3
Hypothyroidism	5	1	3	1
Muscular and joint injury	3	0	2	1
Hepatitis	1	0	0	1
Fatigue	1	0	0	1
Pancreatitis	1	0	1	0

A total of 38 immune-related adverse events occurred in 46 patients.

In the present study, we integrated proteomic and metabolomic profiling of plasma samples from older patients with NSCLC who received anti-PD-1 antibodies to explore potential metabolic biomarkers for irAEs and to understand the development of irAEs in older patients with NSCLC. Our results significantly contribute to the safety management of immunotherapy in older patients with NSCLC.

RESULTS

Patients' characteristics

The study cohort consisted of 46 older patients with stage III-IV NSCLC who were receiving PD-1 inhibitors. A total of 103 blood samples (46 with pre-treatment, 45 with after 1–2 cycles, and 12 with the onset of ≥grade 2 (G2) irAEs) were collected from 46 older patients. The median patient age was 70 years (range: 65–82 years; interquartile range: 67–74 years). The median follow-up was 19.2 months (range: 3.9–42.6 months). All patients who did not develop irAEs completed at least 2 cycles of treatment. Overall, 22 (47.8%) patients had ≥G2 irAEs and 11 (23.9%) had ≥grade 3 (G3) irAEs. None of the patients experienced toxic death (grade 5). The most common irAEs were interstitial pneumonia, dermatological toxicity, and hypothyroidism with rates of 32.6%, 26.1%, and 10.9%, respectively (Table 1). For further data analysis, patients with G2-4 irAEs were defined as the irAE group (n = 22) and patients with G0-1 irAEs (n = 24) were defined as the control group. No significant differences were found in sex, smoking, pathologic type, treatment cycles, and other clinical parameters between the control group and the irAE group (Table S1).

Immunological analysis

Although the specific mechanisms responsible for irAE development have not been fully identified, the potential mechanisms may mimic pathologies of autoimmune disease.[22] Therefore, we quantified the immune factors and lymphocyte subsets in the study cohort at baseline to explore the association between irAEs and immune regulation. For the analysis of immune factors, 59 immune factors, including cytokines, chemokines, growth factors, and immune-oncology checkpoints, were tested in the plasma of the 46 patients (Table S2). However, 13 immune factors with detection rates lower than 20% and one patient (without any irAEs) with significant outliers were excluded from the subsequent analyses. Therefore, 46 immune factors were analyzed in 45 patients (Figure 1A). The results showed that the level of costimulatory receptor CD28 in patients with G2-4 and G3-4 irAEs was significantly lower than that in patients with G0-1 or G0-2 irAEs, respectively. Furthermore, the levels of the immunosuppressive factors IL-10 and CCL2 in patients with G0-2 irAEs were significantly higher than those in patients with G3-4 irAEs (Figure 1B). For the analysis of lymphocyte subsets, 23 patients in our study cohort underwent peripheral blood lymphocyte subset analysis. Significantly lower levels of total T cells, $CD4^+$ T cells, $CD8^+$ T cells, NK cells, and B cells were found in patients with G2-4 or G3-4 irAEs, and statistically significant differences were found in $CD4^+$ T cells (p = 0.031) and B cells (p = 0.002) (Figures 1C and 1D). Our findings suggest an immunocompromised state in older patients who develop ≥G2 irAEs.

Plasma proteomic profiling at baseline

We then performed data-independent acquisition (DIA) proteomic analysis of the plasma samples of the enrolled patients. A total of 5,164 proteins were identified, and no difference in the number of proteins was found between the control and irAE groups (Figure S1). We performed differential protein expression analysis and found 188 proteins that were significantly differentially expressed between the control and irAE groups at baseline (Figure 2A). Principal-component analysis (PCA) was performed to describe the differential profiles between the two groups (Figure 2B). Among the differentially expressed proteins, 132 proteins were upregulated and 56 proteins were downregulated in the irAE group (Figure 2C). ZNF98, ADGRG6, IFT88, ACTN1, and ADH1B were the top five proteins with the most significant p values.

Differentially expressed proteins were selected for Gene Ontology (GO) and Kyoto Encyclopedia of Genes and Genomes (KEGG) pathway analyses. GO analysis revealed three basic functional categories: biological process (BP), molecular function (MF), and cellular component (CC) (Figure S2). In the part of BP, the enriched GO terms were associated with metabolism regulation and inflammatory response, including "fructose 1,6-bisphosphate metabolic process," "glucose catabolic process to pyruvate," "regulation of leukocyte chemotaxis," "response to interleukin-7," and "cell chemotaxis." KEGG pathway analysis further revealed several metabolism-related pathways, such as "Glycolysis/Gluconeogenesis," "Phosphatidylinositide 3 kinases-protein kinase B (PI3K-Akt) signaling pathway," and "Pentose

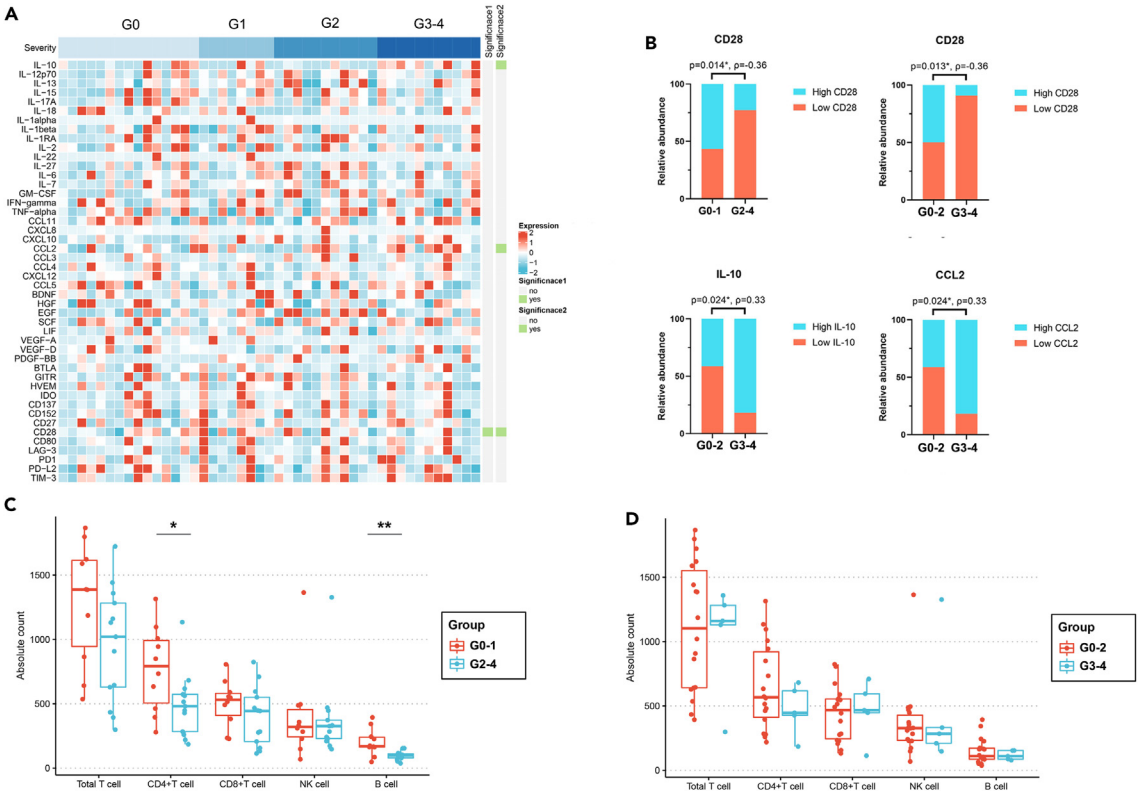

Figure 1. Comparative analysis of immune factors and lymphocyte subsets between control group and irAE group at baseline

(A) Heatmap of 46 immune factors in 45 patients. Significance1 was compared between patients with G0-1 and G2-4 irAEs. Significance2 was compared between patients with G0-2 and G3-4 irAEs (n = 45). Chi-squared test was used for comparison. The cutoffs of immune factors were determined using the median.

(B) Different levels of immune factors included CD28, IL-10, and CCL2.

(C and D) Different absolute counts of lymphocyte subsets were compared between patients with G0-1 and G2-4 irAEs and patients with G0-2 and G3-4 irAEs, respectively (n = 23). G = grades of irAEs. *$p < 0.05$, **$p < 0.01$.

phosphate pathway," which were downregulated in the irAE group, indicating the significance of glucose metabolism in immunotherapy-related toxicities (Figure 2D). In addition, glycosylation-related pathways, including "N-Glycan biosynthesis" and "Other types of O-glycan biosynthesis" were upregulated in the irAE group. The differentially expressed proteins involved in glycolysis and glycosylation-related pathways were aldolase, fructose-bisphosphate B (ALDOB), and ST6 beta-galactoside alpha-2,6-sialyltransferase 1 (ST6GAL1). The expression of these two proteins in the two groups is shown in Figures 2E and 2F.

Plasma metabolomic profiling at baseline

The aforementioned results suggest different metabolic regulation between the control and irAE groups at baseline. To further identify different metabolic regulations between the two groups, pre-treatment plasma was subjected to liquid chromatography-tandem mass spectrometer/mass spectrometry (LC-MS/MS). As a result, 652 metabolites were detected in the positive mode (electrospray ionization, ESI+) and 534 metabolites were detected in the negative mode (ESI−). Supervised orthogonal partial least-squares discriminant analysis (OPLS-DA) was introduced to characterize the metabolomic differences between the two groups in both ESI+ and ESI−, suggesting an association between plasma metabolites and irAEs (Figure 3A). Permutation test and 7-fold cross-validation showed the reliability of the model (Figure S3). The top three largest metabolite classes were lipid and lipid-like molecules (28.921%), organic acids and derivatives (20.995%), and organo-heterocyclic compounds (10.793%) (Figure 3B).

A total of 33 metabolites with $p < 0.05$ and variable importance in the projection (VIP) >1 were considered different. Among these, 14 metabolites were upregulated and 19 metabolites were downregulated in the irAE group (Figure S4A). Heatmaps of the differentially expressed glucose, amino acids, and lipids are shown in Figures S4B–S4D. Of these, a significantly lower lactate/pyruvate ratio was found in the irAE group (p = 0.032), while plasma lactate and pyruvate levels did not differ between the groups (Figure 3C). Kynurenine, tryptophan, and the kynurenine/tryptophan ratio were reported to be closely associated with the antitumor effect of immunotherapy,[23] while they were not associated with irAEs in our study (Figure 3D). However, leucine, lsodeoxycholic acid, and lathosterol were significantly different between the two groups (Figures 3E and 3F). These results indicated different plasma metabolomic profiles in patients with irAEs.

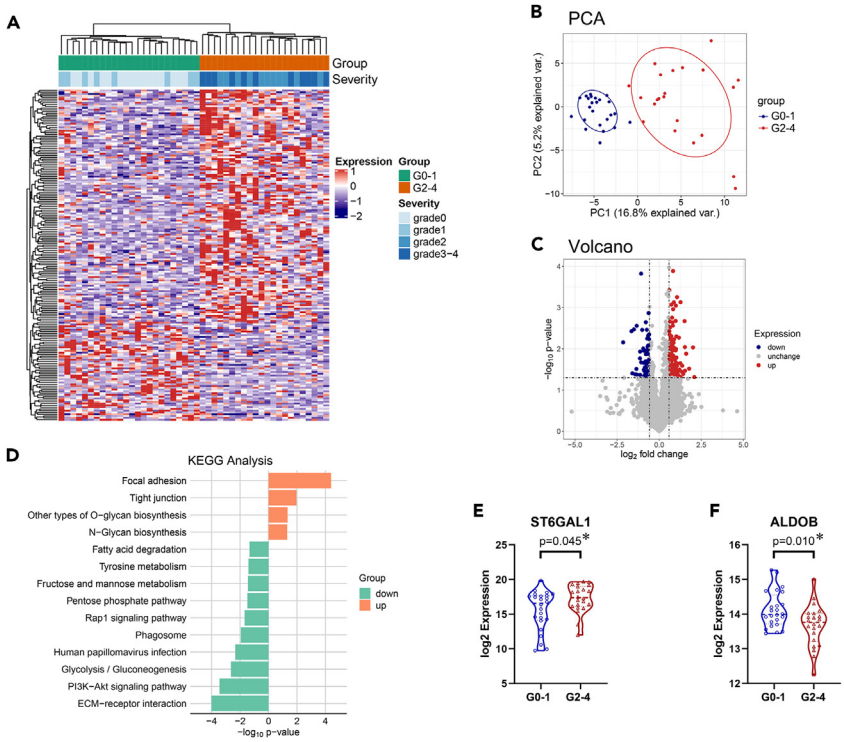

Figure 2. Proteomic differences associated with irAEs at baseline (n = 46)

(A) Heatmap of differently expressed proteins between control group (n = 24) and irAE group (n = 22) ($p < 0.05$, FC > 1.5 or FC < 0.67).

(B) PCA of the differently expressed proteins between control group and irAE group.

(C) Volcano plot representation of the differently expressed proteins between control group and irAE group. (D) KEGG analysis of differently expressed proteins. (E and F) Different expression of ST6GAL1 and ALDOB between control group and irAE group (*$p < 0.05$). G = grades of irAEs; PCA, principal-component analysis; FC, fold change; KEGG, Kyoto Encyclopedia of Genes and Genomes; FC, fold change.

We then performed KEGG pathway analysis for the differentially expressed metabolites. Several metabolism-related pathways, such as glutathione metabolism, galactose metabolism, and lysine degradation, were enriched, and the top 15 functionally enriched KEGG pathways are shown in Figure 3G. The PI3K/AKT/mammalian target of rapamycin (mTOR) signaling pathway is implicated in the metabolic regulation of local nutrients and systemic energy status at organismal and cellular level.[24] We identified that the PI3K/AKT/mTOR signaling pathway was enriched in both KEGG analyses of differentially expressed proteins and metabolites. These results indicated that different metabolic mechanisms may be involved in the development of irAEs.

Severity and temporal dynamics analysis of glycolysis and glycosylation in irAEs

The importance of glycolysis in T cell survival and the involvement of glycolysis in the regulation of the cancer immune response have been investigated.[25] Glycosylation has also been reported to play a vital role in cancer immune response.[26] Therefore, we investigated the severity and temporal dynamics of glycolysis-associated molecules, including ALDOB, lactate/pyruvate ratio, and glycosylation-associated molecule ST6GAL1, in the development of irAEs.

ALDOB expression (p = 0.011) and lactate/pyruvate ratio (p = 0.033) showed a significant decreasing trend with irAE severity (Figures 4A and 4B). ST6GAL1 expression increased with irAE severity, but this was not statistically significant (p = 0.082) (Figure 4C). These results suggest that ALDOB expression and the lactate/pyruvate ratio could predict the severity of irAEs and the impact of glycolysis on the development of irAEs.

Next, we assessed how these plasma biomarkers changed with the development of irAEs. First, we employed the fuzzy c-means algorithm to analyze the trend in plasma protein expression over time (baseline-after 1–2 cycles-onset of irAEs) in 12 patients who developed ≥G2 irAEs. The trends in protein expression were grouped into nine types. Clusters 3, 6, and 9 were considered upregulated proteins, while clusters 1, 4, and 7 were considered downregulated proteins (Figure S5). KEGG analysis was performed separately for upregulated and downregulated proteins. The results revealed that upregulated protein were enriched in diverse metabolic pathways, such as "Cholesterol metabolism," "Pentose phosphate pathway," "Glycolysis/Gluconeogenesis," and "PI3K-Akt signaling pathway" (Figure 4D). Downregulated proteins were enriched in the glycosylation pathway, such as "N-Glycan biosynthesis" and "Various types of N-glycan biosynthesis" (Figure 4E). The detailed temporal dynamics of ALDOB, the lactate/pyruvate ratio, and ST6GAL1 are shown in Figures 4F–4H. Next, we compared the

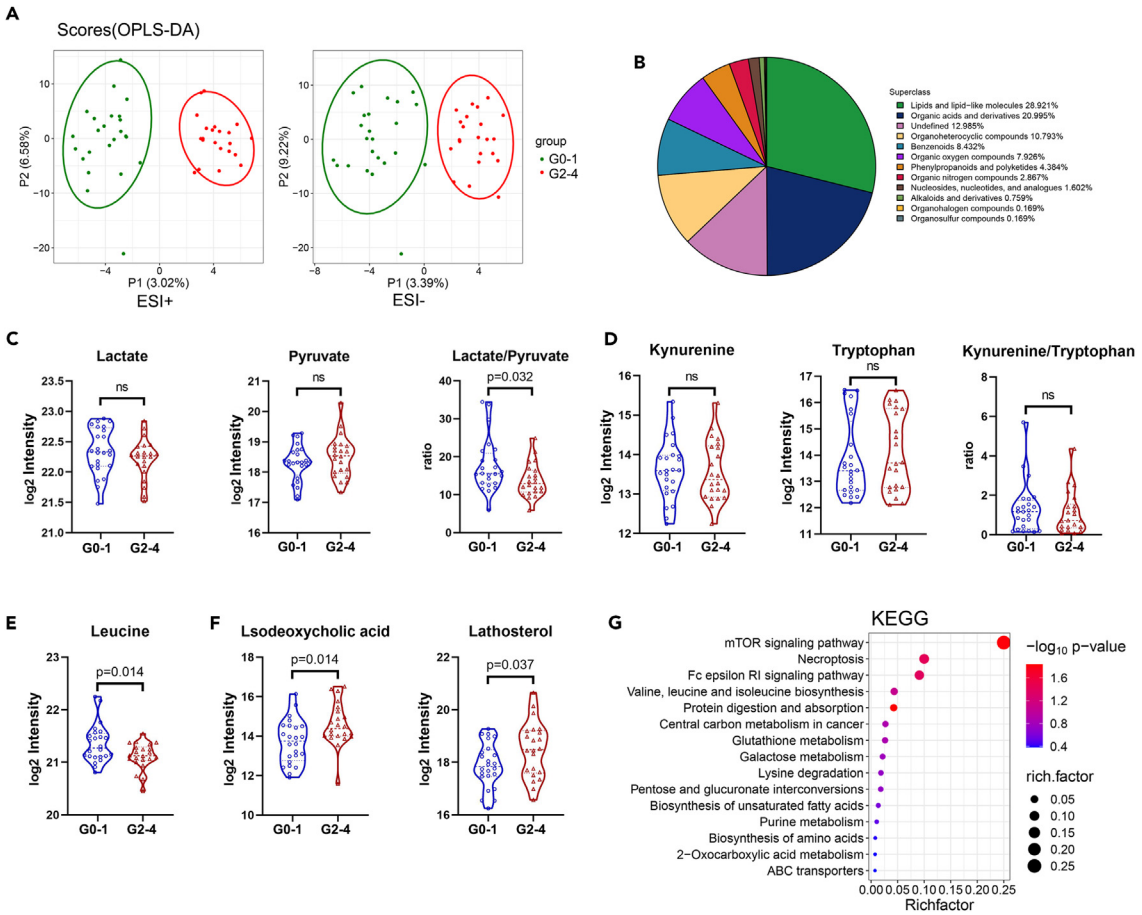

Figure 3. Metabolomic differences associated with irAEs at baseline (*n* = 46)

(A) OPLS-DA of ESI+ and ESI− modes between control group and irAE group.

(B) Proportion of metabolites regulated in all patients based on superclass.

(C–F) Vital metabolites compared between control group and irAE group.

(G) KEGG analysis of differently changed metabolites ($p < 0.05$, VIP >1). G = grades of irAEs; KEGG, Kyoto Encyclopedia of Genes and Genomes; ns, no significance.

early changes (baseline-after 1–2 cycles) of these molecules between the control and irAE groups. In the irAE group, treatment induced a significant increase in ALDOB ($p = 0.004$) and a significant decrease in ST6GAL1 ($p = 0.026$), with no significant change in the lactate/pyruvate ratio ($p = 0.542$) (Figures 4I–4K). These results suggest that increased glycolysis and decreased glycosylation are involved in the development of irAEs. Furthermore, these changes could be tested in the early stages of irAE development and predicted a higher risk of irAEs.

Metabolic biomarkers of high diagnostic value in predicting irAEs

Ensemble learning methods based on metabolic profiling were used to verify the relevance of the identified metabolites in the occurrence of ≥G2 irAEs. Fifty-seven significantly different metabolites with $p < 0.1$ and VIP >1 between the ≥G2 irAE group and the control group were included in the analysis. The entire cohort was divided into a training group and a testing group at a ratio of 7:3. In the training group, the differentially expressed metabolites were sorted from high to low according to the weight values calculated using the ensemble learning methods. The top 10 metabolites were then used to generate the receiver operating characteristic (ROC) accumulating curves, and the combination of MT171T257, M219T111, M604T33, and M146T49 was selected (Figures 5A and 5B). A logistic regression model was built with the aforementioned biomarkers showing a high value in distinguishing patients with ≥G2 irAEs from those with G0-1 irAEs by ROC curve analysis (training group: AUC = 0.831, testing group: AUC = 0.976, Figure 5C).

Since grade 3–4 irAEs indicate permanent suspension of ICIs, a further distinction of ≥G3 irAEs is necessary. Therefore, we identified seventy-eight significantly different metabolites ($p < 0.1$ between patients with G2 irAEs [$n = 11$] and those with ≥G3 irAEs [$n = 11$]. A cohort of twenty-two patients with ≥G2 irAEs was assigned to the training and testing groups in a ratio of 7:3. In the training group, a total of eight metabolites, including M219T111, M595T216, M647T389, M413T111, M119T429, M564T275_1, M405T101, and M279T48, were determined using ensemble learning methods and ROC accumulating curves (Figures 5D and 5E). The aforementioned metabolites based on the logistic

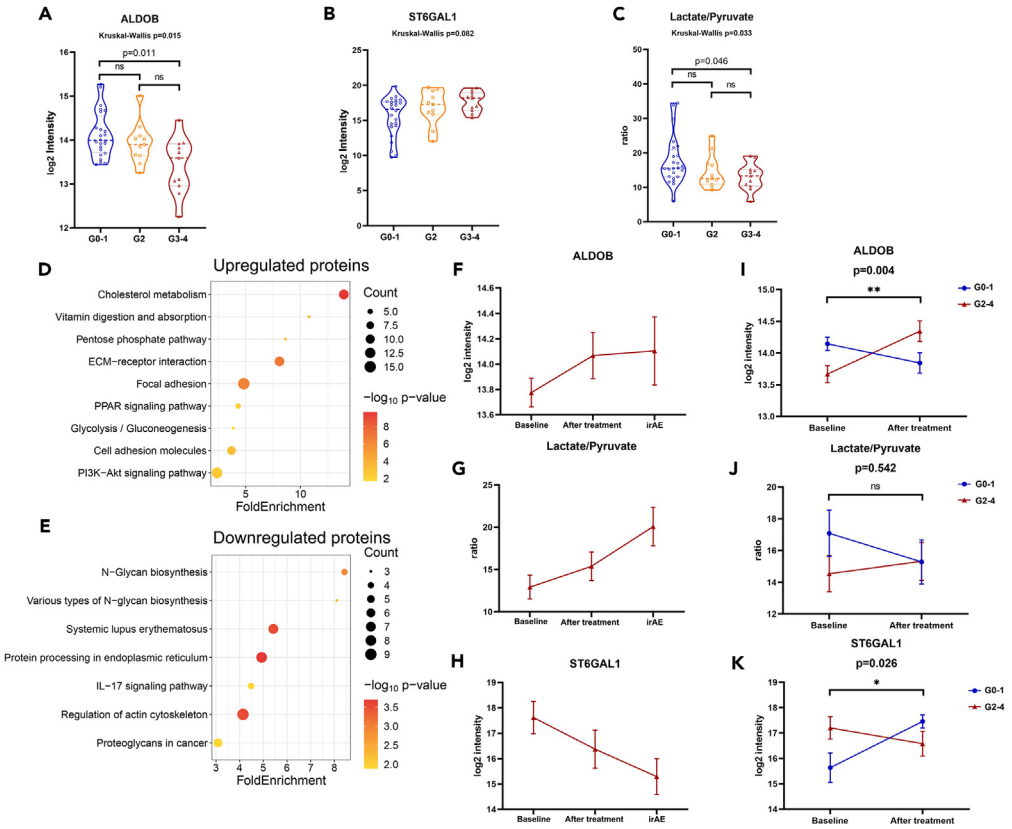

Figure 4. Severity and temporal dynamics analysis of proteins and metabolites in patients treated with ICIs

(A–C) The change trend of ALDOB, ST6GAL1, and lactate/pyruvate ratio associated with severity of irAEs (n = 46). Kruskal-Wallis tests were used for multi-group comparisons, and Bonferroni was used for pairwise comparisons.

(D and E) KEGG analysis of upregulated proteins and downregulated proteins during the development of ≥G2 irAEs (n = 12).

(F–H) The change trend of expression of ALDOB, lactate/pyruvate, and ST6GAL1 during the development of ≥G2 irAEs (n = 12).

(I–K) Significant changes of ALDOB, lactate/pyruvate, and ST6GAL1 before and after treatment with 1–2 cycles of ICIs (n = 24/control group, n = 21/irAE group). Statistical significance was determined by two-tailed Wilcoxon signed-rank test. Baseline: at baseline; After: after 1–2 cycles of ICIs; On, the onset of irAEs. ICI, immune checkpoint inhibitor; G = grades of irAEs; ns, no significance. *p < 0.05, **p < 0.01.

regression model were verified as excellent in distinguishing patients with G3-4 irAEs from patients with G2 irAEs by ROC curve analysis (training group: AUC = 1, testing group: AUC = 1, Figure 5F). Detailed information on these metabolites is provided in Tables S3 and S4.

ALDOB and lactate/pyruvate ratio correlate with prognosis of ICIs

There was no significant association between clinical responses and ALDOB expression, lactate/pyruvate ratio, and ST6GAL1 expression (Figures 6A–6C). Subsequently, we compared the survival prognosis between patients with low and high ALDOB expression, lactate/pyruvate ratio, and ST6GAL1 expression. Patients with low ALDOB expression or lactate/pyruvate ratio had a longer progression-free survival (PFS) than those with high expression (mPFS: ALDOB, 14.6 months vs. 8 months, p = 0.046; lactate/pyruvate ratio, 13 months vs. 6.2 months, p = 0.001, Figures 6D and 6E). However, no significant difference in PFS was observed between patients with low and high ST6GAL1(Figure 6F). Multivariate analysis considering pathologic type, tumor stage, treatment regimen, etc. revealed that the expression of ALDOB (Hazard ratio, HR = 2.248, p = 0.037), lactate/pyruvate ratio (HR = 2.518, p = 0.016), and number of treatment cycles (HR = 0.913, p = 0.013) were independent prognostic factors for PFS in older patients with NSCLC (Table 2). Furthermore, we compared the associations between irAEs and treatment outcomes in the study cohort. The results showed that the clinical response and PFS were not associated with the occurrence of irAEs (Figure S6).

DISCUSSION

Older adults, as a particular cohort with dysregulated immune function, may be more prone to immunotherapy-related toxicities after ICI treatment.[5,6] Cell metabolism, a crucial determinant in preserving the vitality and function of immune cells, is an effective predictor of ICI response.[19–21] The current study integrated proteomic and metabolomic profiling to discover plasma metabolism-related biomarkers

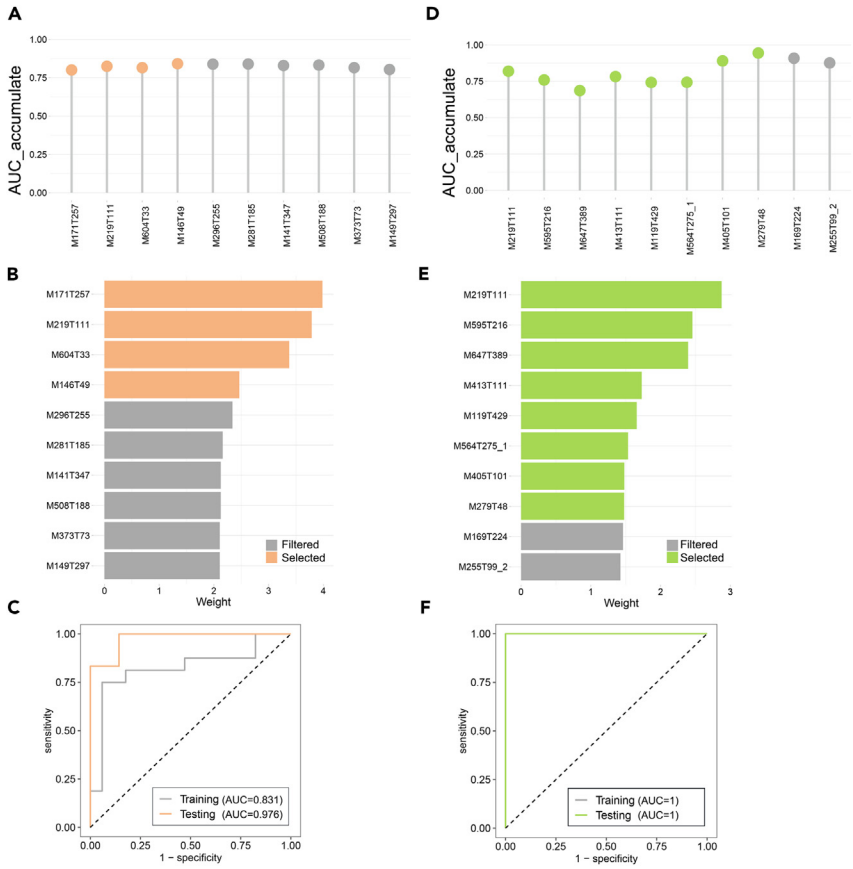

Figure 5. Discovery of the metabolic biomarkers for irAEs

(A–C) Metabolic biomarkers for ≥ G2 irAEs (n = 22) vs. G0-1 irAEs (n = 24): (A) the cumulative AUC of the differently expressed metabolites between ≥ G2 irAEs and G0-1 irAEs; (B) the top 10 metabolites in weight score between ≥ G2 irAEs and G0-1 irAEs; (C) ROC curve of the selected metabolites between ≥G2 irAEs and G0-1 irAEs.

(D–F) Metabolic biomarkers for G2 irAEs (n = 11) vs. ≥G3 irAEs (n = 11): (D) the cumulative AUC of the differently expressed metabolites between G2 irAEs and ≥G3 irAEs; (E) the top 10 metabolites in importance score between G2 irAEs and ≥G3 irAEs; (F) ROC curve of the selected metabolites between G2 irAEs and ≥G3 irAEs.

associated with irAEs. Additionally, we used ensemble learning methods and logistic regression to establish a metabolism-relevant predictive model for irAEs with a high diagnostic value. Furthermore, we found lower expression of ALDOB or a lower lactate/pyruvate ratio indicates a favorable prognosis of ICI treatment in older patients with NSCLC.

Many studies have explored lymph subsets and cytokines as predictive biomarkers for irAEs, indicating a pre-existing active immunological and inflammatory system in individuals who develop irAEs.[27,28] However, older patients undergoing ICI treatment are potentially important because of immune dysfunction, but few studies have concentrated on this. PD-1-mediated suppression is more likely to target the T cell costimulatory receptor CD28.[29] The CD28 molecule expressed in activated T cells is proteolytically degraded by matrix metalloproteinase (MMP) 2 and MMP 13, resulting in increased plasma soluble CD28 (sCD28) levels. Previous studies have shown that plasma sCD28 levels were increased in patients with autoimmune diseases, such as antineutrophil cytoplasmic antibody (ANCA)-associated vasculitis[30] and early rheumatoid arthritis,[31] indicating immunoactivation of sCD28. Another study confirmed the function of sCD28 in stimulating T cell responses.[32] Our findings revealed that the sCD28 levels were significantly lower at baseline in older individuals with irAEs. Furthermore, IL-10 and CCL2, which function as immunosuppressive factors,[33,34] significantly increased in the irAE group. These results suggest that the pre-treatment immunocompromised state could be related to the occurrence of irAEs in older patients with NSCLC.

Cell metabolism determines the fate of the immune cells. Compared with conventional flow cytometry to detect the quantity of antigen-specific immune cells, changes in metabolic regulation in peripheral blood may be a better measure to evaluate immune regulation. In this study, we used proteomic and metabolomic profiling to reveal that multiple metabolism-related pathways, including glycolysis, pentose phosphate pathway, and PI3K/Akt signaling pathway, were downregulated at baseline in patients with irAEs. Furthermore, patients with irAEs had significantly lower lactate/pyruvate ratios, which also exhibited a significantly decreasing trend as irAE severity increased. Glycolysis is

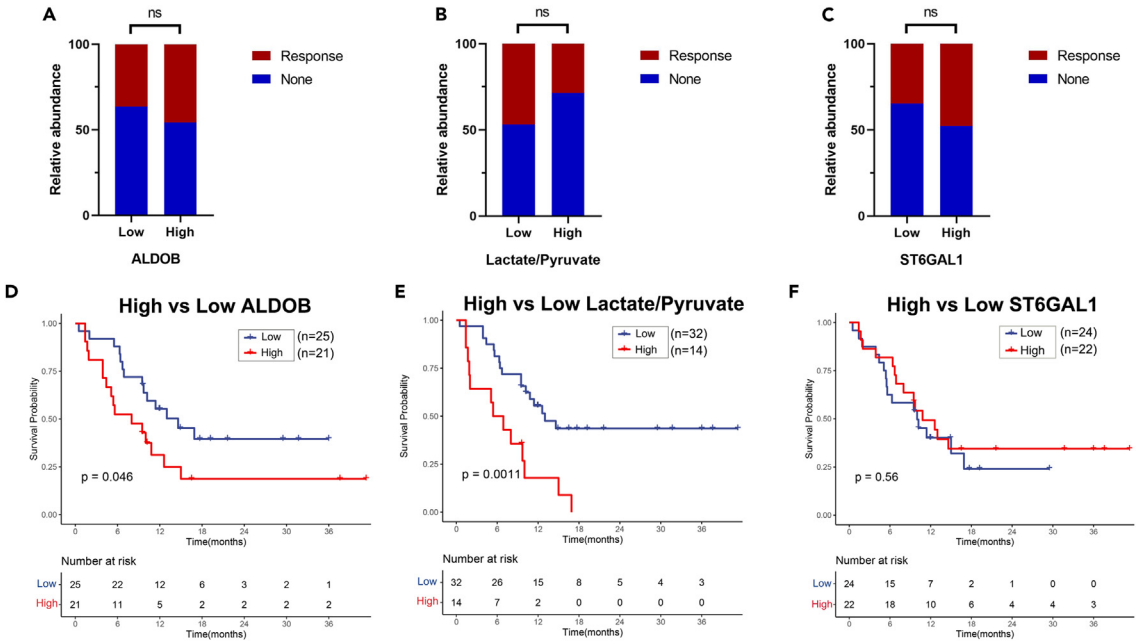

Figure 6. Association of efficacy of ICIs with ALDOB, lactate/pyruvate ratio, and ST6GAL1 (*n* = 46)

(A–C) Association of clinical outcomes with the expression of (A) ALDOB, (B) lactate/pyruvate ratio, and (C) ST6GAL1. The cutoff of high or low level was determined by the maximum Youden index value.

(D–F) Kaplan-Meier curves of PFS between patients with high and low expression of (D) ALDOB, (E) lactate/pyruvate ratio, and (F) ST6GAL1. Log rank tests were used to evaluate survival differences. PFS, progression-free survival; ns, no significance.

crucial for T cell activation, and CD28 activation is required to activate glycolytic metabolism.[35] Therefore, our metabolomic results suggest decreased glycolysis and an immunocompromised state at baseline in patients with irAEs, consistent with our immunological analysis. ALDOB, a protein that was significantly downregulated in the irAE group, is involved in glycolysis by converting fructose phosphate into glyceraldehyde and dihydroxyacetone phosphate. According to a recent study, hepatic ALDOB reduced hepatocellular tumorigenesis by inhibiting Akt.[36] However, the involvement of ALDOB in immunological modulation has not been reported. Further studies with larger sample sizes are needed to verify the relationship between ALDOB and irAEs.

Glycosylation leads to the formation of glycans on the cell surface and regulates T cell activation and function. In most cases, glycosylation of immune cells prevents immune overactivation, while glycosylation of tumor cells contributes to immune escape. For instance, glycans on CD28 inhibit T cell activation,[37] and glycosylated PD-L1 in human tumor tissues can stabilize the PD-L1 protein, promoting immunological tolerance.[38] Aberrant glycosylation is associated with autoimmune diseases.[39] Our results showed an upregulated glycosylation pathway and glycosylation enzyme ST6GAL1 at baseline in patients with irAEs, but they did not identify the precise glycosylation site or the precise cell type that was glycosylated. Detection of glycosylation at the single-cell level is required to investigate the mechanisms of irAE development.

The occurrence of irAEs is caused by ICIs that destroy immune tolerance. Therefore, early changes between pre- and post-treatment are important for predicting irAEs.[40,41] In this study, we revealed that the early changes of ALDOB and ST6GAL1 between pre- and post-treatment were significantly associated with the development of irAEs, and the longitudinal tracking of plasma proteins in twelve patients with G2-4 irAEs indicated an upregulated glycolysis pathway and downregulated glycosylation pathway, which was consistent with the early changing trends of ALDOB and ST6GAL1, respectively. The lactate/pyruvate ratio showed an increasing trend in the early stage in the irAE group compared with that in the control group, but the difference was not statistically significant. We suspect that this may be because changes in metabolic enzymes precede changes in metabolites during the development of irAEs. Notably, the baseline levels of ALDOB and ST6GAL1 were opposite to their early changing trends, suggesting that patients with irAEs display an immunocompromised state at baseline but immune overactivation after the initial use of ICIs.

In addition, we found that the integration of these differently expressed metabolites at baseline based on ensemble learning methods and logistic regression allowed for a high diagnostic value for the classification between patients with G2-4 irAEs and G0-1 irAEs, and between patients with G3-4 irAEs and G2 irAEs. Studies on these metabolites in models are relatively rare. Oleic acid, *cis*,*cis*-muconic acid, and linoleic acid are involved in fatty acid metabolism. Gallic acid was identified from gut microbial metabolites, decreasing T_{reg} cell function by impairing PD-L1/PD-1 signaling and downregulating Foxp3 stability.[42] Nevertheless, these results implicate the role of metabolites in predicting the occurrence of irAEs and the involvement of metabolic regulation in the development of irAEs. Our prediction models may provide clinical guidance for older patients undergoing tumor immunotherapy.

Table 2. Univariate and multivariate analyses of progression-free survival (*n* = 46)

	Univariate analysis			Multivariate analysis		
Characteristics	HR	95% CI	P	HR	95% CI	P
Age	0.945	0.870–1.027	0.182			
Sex (male vs. female)	0.966	0.369–2.528	0.943			
Smoking (no vs. yes)	0.816	0.423–1.571	0.542			
Pathologic type (LUAD vs. LUSC vs. others)	1.247	0.732–2.126	0.417			
Stage (M0 vs. M1)	1.330	0.589–3.004	0.493			
Combination therapy (no vs. yes)	2.056	0.622–6.793	0.237			
Line of treatment (first-line vs. second-line or more)	0.988	0.379–2.583	0.980			
Expression of PD-L1 (<1 vs. NA vs. ≥ 1)	1.048	0.653–1.683	0.845			
ECOG score (<2 vs. ≥ 2)	1.305	0.309–5.513	0.717			
Number of treatment cycles	0.918	0.858–0.982	**0.013**	0.913	0.849–0.981	**0.013**
ALDOB (low vs. high)	2.065	1.001–4.260	**0.049**	2.248	1.050–4.812	**0.037**
Lactate/Pyruvate (low vs. high)	3.188	1.526–6.660	**0.002**	2.518	1.190–5.328	**0.016**
ST6GAL1 (low vs. high)	0.845	0.413–1.733	0.646			

LUAD, lung adenocarcinoma; LUSC, lung squamous cell carcinoma; ECOG, Eastern Cooperative Oncology Group.

Although the full mechanism of irAEs is not clear, it is accepted that irAEs may occur at higher rates in patients with immune dysregulation.[43] Senescent T cells are thought to be characterized by impaired immune function, thereby acting as a major cause of the higher rates of irAEs in older patients. For example, senescent Temra $CD8^+$ cells were significantly increased in the blood of patients with immune-related myocarditis, corresponding to an analogous increase in effector cytotoxic $CD8^+$ cells in the hearts of mice with myocarditis.[44] However, recent studies have found that senescent T cells could be affected by T_{reg} cells and tumor cells, except for the age,[45] indicating that the age could not determine the degree of immune senescence. Furthermore, senescent T cells display lower CD28[46] expression and reduced glycolysis,[47] implying that peripheral blood metabolomics may be a good alternative for describing the degree of immune senescence. Surprisingly, we found that low ALDOB expression and low lactate/pyruvate ratio were independent factors for a favorable prognosis. This suggests that glycolysis-related biomarkers could help guide clinical decision making for immunotherapy in older patients with NSCLC.

To conclude, we showed different plasma metabolic regulations between older patients with NSCLC who developed irAEs and those who did not. Lower ALDOB, lower lactate/pyruvate ratio, and higher ST6GAL1 at baseline as well as early changes in ALDOB and ST6GAL1 expression were predictors of irAEs. Furthermore, predictive models were developed with a high diagnostic value based on metabolic markers to evaluate the occurrence of G2-4 and G3-4 irAEs in older patients with NSCLC. We also found lower ALDOB expression and a lower lactate/pyruvate ratio indicating a good prognosis in older patients with NSCLC. Given that lower CD28 and higher IL-10 and CCL2 levels were associated with irAEs, our results suggest a potential pre-treatment immunocompromised state, which could be the trigger of irAEs in older patients. Therefore, these could be significant findings to provide a comprehensive approach to help for insight into the risk stratification of older patients with NSCLC before ICI treatment to improve the safety of immunotherapy.

Limitations of the study

This study has limitations in interpreting our findings. First, we did not verify the relationship between metabolic regulation and irAEs in specific cells, since plasma metabolites could be produced by various types of cells, such as immune cells, tumor cells, and even gut microbiota. Single-cell RNA sequencing is required to verify the metabolic regulation of immune cells. Second, although untargeted metabolomics can comprehensively analyze changes of all metabolites, it cannot accurately analyze some specific metabolic pathways, such as lipid metabolism, which also contribute to the activation and proliferation of immune cells. Follow-up targeted metabolomics is needed to explore into specific metabolic pathways. Third, there is the possibility of selection bias due to small sample size. Larger cohort will be necessary to confirm the aforementioned results.

STAR★METHODS

Detailed methods are provided in the online version of this paper and include the following:

- KEY RESOURCES TABLE
- RESOURCE AVAILABILITY
  - Lead contact

SUPPLEMENTAL INFORMATION

Supplemental information can be found online at https://doi.org/10.1016/j.isci.2024.109946.

ACKNOWLEDGMENTS

The authors wish to acknowledge the support of the Shanghai Applied Protein Technology Co., Ltd. We acknowledge the technical contributions of Liuya Yang in the Metabolomic Department, Chenxi Wei in the Proteomic Department, and Jie Tang in the Bioinformatics Department. The authors thank the patients and their families who agreed to participate in this study.

This work was supported by CAMS Innovation Fund for Medical Sciences (2021-I2M-1-012).

AUTHOR CONTRIBUTIONS

J.G., P.Z., M.T., X.N., and L.L. contributed to the conception and design of this study. The data collection was completed by Y.Y. and X.W. Sample collection was completed by J.M. Formal analysis and the original draft were completed by J.G. Funding was obtained from L.L., and she supervised the manuscript. All authors have read and agreed to the published version of the manuscript.

DECLARATION OF INTERESTS

The authors declare no competing interests.

Received: July 5, 2023
Revised: December 12, 2023
Accepted: May 6, 2024
Published: May 8, 2024

REFERENCES

1. Pillai, R.N., Behera, M., Owonikoko, T.K., Kamphorst, A.O., Pakkala, S., Belani, C.P., Khuri, F.R., Ahmed, R., and Ramalingam, S.S. (2018). Comparison of the toxicity profile of PD-1 versus PD-L1 inhibitors in non-small cell lung cancer: A systematic analysis of the literature. Cancer *124*, 271–277.
2. Miller, K.D., Nogueira, L., Devasia, T., Mariotto, A.B., Yabroff, K.R., Jemal, A., Kramer, J., and Siegel, R.L. (2022). Cancer treatment and survivorship statistics, 2022. CA Cancer J. Clin. *72*, 409–436.
3. Reck, M., Rodríguez-Abreu, D., Robinson, A.G., Hui, R., Csőszi, T., Fülöp, A., Gottfried, M., Peled, N., Tafreshi, A., Cuffe, S., et al. (2019). Updated Analysis of KEYNOTE-024: Pembrolizumab Versus Platinum-Based Chemotherapy for Advanced Non-Small-Cell Lung Cancer With PD-L1 Tumor Proportion Score of 50% or Greater. J. Clin. Oncol. *37*, 537–546.
4. Mok, T.S.K., Wu, Y.L., Kudaba, I., Kowalski, D.M., Cho, B.C., Turna, H.Z., Castro, G., Jr., Srimuninnimit, V., Laktionov, K.K., Bondarenko, I., et al. (2019). Pembrolizumab versus chemotherapy for previously untreated, PD-L1-expressing, locally advanced or metastatic non-small-cell lung cancer (KEYNOTE-042): a randomised, open-label, controlled, phase 3 trial. Lancet *393*, 1819–1830.
5. Rodrigues, L.P., Teixeira, V.R., Alencar-Silva, T., Simonassi-Paiva, B., Pereira, R.W., Pogue, R., and Carvalho, J.L. (2021). Hallmarks of aging and immunosenescence: Connecting the dots. Cytokine Growth Factor Rev. *59*, 9–21.
6. Rodriguez, J.E., Naigeon, M., Goldschmidt, V., Roulleaux Dugage, M., Seknazi, L., Danlos, F.X., Champiat, S., Marabelle, A., Michot, J.M., Massard, C., et al. (2022). Immunosenescence, inflammaging, and cancer immunotherapy efficacy. Expert Rev. Anticancer Ther. *22*, 915–926.
7. Baldini, C., Martin Romano, P., Voisin, A.L., Danlos, F.X., Champiat, S., Laghouati, S., Kfoury, M., Vincent, H., Postel-Vinay, S., Varga, A., et al. (2020). Impact of aging on immune-related adverse events generated by anti-programmed death (ligand)PD-(L)1 therapies. Eur. J. Cancer *129*, 71–79.
8. Fujimoto, D., Miura, S., Yoshimura, K., Wakuda, K., Oya, Y., Haratani, K., Itoh, S., Uemura, T., Morinaga, R., Takahama, T., et al. (2022). A Real-World Study on the Effectiveness and Safety of Pembrolizumab Plus Chemotherapy for Nonsquamous NSCLC. JTO Clin. Res. Rep. *3*, 100265.
9. Morimoto, K., Yamada, T., Yokoi, T., Kijima, T., Goto, Y., Nakao, A., Hibino, M., Takeda, T., Yamaguchi, H., Takumi, C., et al. (2021). Clinical impact of pembrolizumab combined with chemotherapy in elderly patients with

advanced non-small-cell lung cancer. Lung Cancer *161*, 26–33.
10. Nebhan, C.A., Cortellini, A., Ma, W., Ganta, T., Song, H., Ye, F., Irlmeier, R., Debnath, N., Saeed, A., Radford, M., et al. (2021). Clinical Outcomes and Toxic Effects of Single-Agent Immune Checkpoint Inhibitors Among Patients Aged 80 Years or Older With Cancer: A Multicenter International Cohort Study. JAMA Oncol. *7*, 1856–1861.
11. Oh, D.Y., Cham, J., Zhang, L., Fong, G., Kwek, S.S., Klinger, M., Faham, M., and Fong, L. (2017). Immune Toxicities Elicted by CTLA-4 Blockade in Cancer Patients Are Associated with Early Diversification of the T-cell Repertoire. Cancer Res. *77*, 1322–1330.
12. Subudhi, S.K., Aparicio, A., Gao, J., Zurita, A.J., Araujo, J.C., Logothetis, C.J., Tahir, S.A., Korivi, B.R., Slack, R.S., Vence, L., et al. (2016). Clonal expansion of CD8 T cells in the systemic circulation precedes development of ipilimumab-induced toxicities. Proc. Natl. Acad. Sci. USA *113*, 11919–11924.
13. Lozano, A.X., Chaudhuri, A.A., Nene, A., Bacchiocchi, A., Earland, N., Vesely, M.D., Usmani, A., Turner, B.E., Steen, C.B., Luca, B.A., et al. (2022). T cell characteristics associated with toxicity to immune checkpoint blockade in patients with melanoma. Nat. Med. *28*, 353–362.
14. Patel, A.J., Willsmore, Z.N., Khan, N., Richter, A., Naidu, B., Drayson, M.T., Papa, S., Cope, A., Karagiannis, S.N., Perucha, E., and Middleton, G.W. (2022). Regulatory B cell repertoire defects predispose lung cancer patients to immune-related toxicity following checkpoint blockade. Nat. Commun. *13*, 3148.
15. Phillips, G.S., Wu, J., Hellmann, M.D., Postow, M.A., Rizvi, N.A., Freites-Martinez, A., Chan, D., Dusza, S., Motzer, R.J., Rosenberg, J.E., et al. (2019). Treatment Outcomes of Immune-Related Cutaneous Adverse Events. J. Clin. Oncol. *37*, 2746–2758.
16. Wang, H., Zhou, F., Zhao, C., Cheng, L., Zhou, C., Qiao, M., Li, X., and Chen, X. (2022). Interleukin-10 Is a Promising Marker for Immune-Related Adverse Events in Patients With Non-Small Cell Lung Cancer Receiving Immunotherapy. Front. Immunol. *13*, 840313.
17. Watson, M.J., Vignali, P.D.A., Mullett, S.J., Overacre-Delgoffe, A.E., Peralta, R.M., Grebinoski, S., Menk, A.V., Rittenhouse, N.L., DePeaux, K., Whetstone, R.D., et al. (2021). Metabolic support of tumour-infiltrating regulatory T cells by lactic acid. Nature *591*, 645–651.
18. Nishida, M., Yamashita, N., Ogawa, T., Koseki, K., Warabi, E., Ohue, T., Komatsu, M., Matsushita, H., Kakimi, K., Kawakami, E., et al. (2021). Mitochondrial reactive oxygen species trigger metformin-dependent antitumor immunity via activation of Nrf2/mTORC1/p62 axis in tumor-infiltrating CD8T lymphocytes. J. Immunother. Cancer *9*, e002954.
19. Triozzi, P.L., Stirling, E.R., Song, Q., Westwood, B., Kooshki, M., Forbes, M.E., Holbrook, B.C., Cook, K.L., Alexander-Miller, M.A., Miller, L.D., et al. (2022). Circulating Immune Bioenergetic, Metabolic, and Genetic Signatures Predict Melanoma Patients' Response to Anti-PD-1 Immune Checkpoint Blockade. Clin. Cancer Res. *28*, 1192–1202.
20. Ghini, V., Laera, L., Fantechi, B., Monte, F.D., Benelli, M., McCartney, A., Leonardo, T., Luchinat, C., and Pozzessere, D. (2020). Metabolomics to Assess Response to Immune Checkpoint Inhibitors in Patients with Non-Small-Cell Lung Cancer. Cancers *12*, 3574.
21. Kocher, F., Amann, A., Zimmer, K., Geisler, S., Fuchs, D., Pichler, R., Wolf, D., Kurz, K., Seeber, A., and Pircher, A. (2021). High indoleamine-2,3-dioxygenase 1 (IDO) activity is linked to primary resistance to immunotherapy in non-small cell lung cancer (NSCLC). Transl. Lung Cancer Res. *10*, 304–313.
22. Esfahani, K., Elkrief, A., Calabrese, C., Lapointe, R., Hudson, M., Routy, B., Miller, W.H., Jr., and Calabrese, L. (2020). Moving towards personalized treatments of immune-related adverse events. Nat. Rev. Clin. Oncol. *17*, 504–515.
23. Huang, J., Liu, D., Wang, Y., Liu, L., Li, J., Yuan, J., Jiang, Z., Jiang, Z., Hsiao, W.W., Liu, H., et al. (2022). Ginseng polysaccharides alter the gut microbiota and kynurenine/tryptophan ratio, potentiating the antitumour effect of antiprogrammed cell death 1/programmed cell death ligand 1 (anti-PD-1/PD-L1) immunotherapy. Gut *71*, 734–745.
24. Tian, L.Y., Smit, D.J., and Jücker, M. (2023). The Role of PI3K/AKT/mTOR Signaling in Hepatocellular Carcinoma Metabolism. Int. J. Mol. Sci. *24*.
25. Madden, M.Z., and Rathmell, J.C. (2021). The Complex Integration of T-cell Metabolism and Immunotherapy. Cancer Discov. *11*, 1636–1643.
26. Gray, M.A., Stanczak, M.A., Mantuano, N.R., Xiao, H., Pijnenborg, J.F.A., Malaker, S.A., Miller, C.L., Weidenbacher, P.A., Tanzo, J.T., Ahn, G., et al. (2020). Targeted glycan degradation potentiates the anticancer immune response in vivo. Nat. Chem. Biol. *16*, 1376–1384.
27. von Itzstein, M.S., Khan, S., and Gerber, D.E. (2020). Investigational Biomarkers for Checkpoint Inhibitor Immune-Related Adverse Event Prediction and Diagnosis. Clin. Chem. *66*, 779–793.
28. Chennamadhavuni, A., Abushahin, L., Jin, N., Presley, C.J., and Manne, A. (2022). Risk Factors and Biomarkers for Immune-Related Adverse Events: A Practical Guide to Identifying High-Risk Patients and Rechallenging Immune Checkpoint Inhibitors. Front. Immunol. *13*, 779691.
29. Duraiswamy, J., Turrini, R., Minasyan, A., Barras, D., Crespo, I., Grimm, A.J., Casado, J., Genolet, R., Benedetti, F., Wicky, A., et al. (2021). Myeloid antigen-presenting cell niches sustain antitumor T cells and license PD-1 blockade via CD28 costimulation. Cancer Cell *39*, 1623–1642.e20.
30. Pyo, J.Y., Yoon, T., Ahn, S.S., Song, J.J., Park, Y.B., and Lee, S.W. (2022). Soluble immune checkpoint molecules in patients with antineutrophil cytoplasmic antibody-associated vasculitis. Sci. Rep. *12*, 21319.
31. García-Chagollán, M., Ledezma-Lozano, I.Y., Hernández-Bello, J., Sánchez-Hernández, P.E., Gutiérrez-Ureña, S.R., and Muñoz-Valle, J.F. (2020). Expression patterns of CD28 and CTLA-4 in early, chronic, and untreated rheumatoid arthritis. J. Clin. Lab. Anal. *34*, e23188.
32. Liu, Y., Tong, C., Xu, Y., Cong, P., Liu, Y., Shi, L., Shi, X., Zhao, Y., Bi, G., Jin, H., and Hou, M. (2019). CD28 Deficiency Ameliorates Blast Exposure-Induced Lung Inflammation, Oxidative Stress, Apoptosis, and T Cell Accumulation in the Lungs via the PI3K/Akt/FoxO1 Signaling Pathway. Oxid. Med. Cell. Longev. *2019*, 4848560.
33. Naing, A., Infante, J.R., Papadopoulos, K.P., Chan, I.H., Shen, C., Ratti, N.P., Rojo, B., Autio, K.A., Wong, D.J., Patel, M.R., et al. (2018). PEGylated IL-10 (Pegilodecakin) Induces Systemic Immune Activation, CD8(+) T Cell Invigoration and Polyclonal T Cell Expansion in Cancer Patients. Cancer Cell *34*, 775–791.e3.
34. Miyamoto, T., Murakami, R., Hamanishi, J., Tanigaki, K., Hosoe, Y., Mise, N., Takamatsu, S., Mise, Y., Ukita, M., Taki, M., et al. (2022). B7-H3 Suppresses Antitumor Immunity via the CCL2-CCR2-M2 Macrophage Axis and Contributes to Ovarian Cancer Progression. Cancer Immunol. Res. *10*, 56–69.
35. Utley, A., Chavel, C., Lightman, S., Holling, G.A., Cooper, J., Peng, P., Liu, W., Barwick, B.G., Gavile, C.M., Maguire, O., et al. (2020). CD28 Regulates Metabolic Fitness for Long-Lived Plasma Cell Survival. Cell Rep. *31*, 107815.
36. Liu, G., Wang, N., Zhang, C., Li, M., He, X., Yin, C., Tu, Q., Shen, X., Zhang, L., Lv, J., et al. (2021). Fructose-1,6-Bisphosphate Aldolase B Depletion Promotes Hepatocellular Carcinogenesis Through Activating Insulin Receptor Signaling and Lipogenesis. Hepatology *74*, 3037–3055.
37. Ma, B.Y., Mikolajczak, S.A., Yoshida, T., Yoshida, R., Kelvin, D.J., and Ochi, A. (2004). CD28 T cell costimulatory receptor function is negatively regulated by N-linked carbohydrates. Biochem. Biophys. Res. Commun. *317*, 60–67.
38. Li, C.W., Lim, S.O., Chung, E.M., Kim, Y.S., Park, A.H., Yao, J., Cha, J.H., Xia, W., Chan, L.C., Kim, T., et al. (2018). Eradication of Triple-Negative Breast Cancer Cells by Targeting Glycosylated PD-L1. Cancer Cell *33*, 187–201.e10.
39. Ząbczyńska, M., Link-Lenczowski, P., and Pocheć, E. (2021). Glycosylation in Autoimmune Diseases. Adv. Exp. Med. Biol. *1325*, 205–218.
40. Khan, S., Khan, S.A., Luo, X., Fattah, F.J., Saltarski, J., Gloria-McCutchen, Y., Lu, R., Xie, Y., Li, Q., Wakeland, E., and Gerber, D.E. (2019). Immune dysregulation in cancer patients developing immune-related adverse events. Br. J. Cancer *120*, 63–68.
41. Oyanagi, J., Koh, Y., Sato, K., Mori, K., Teraoka, S., Akamatsu, H., Kanai, K., Hayata, A., Tokudome, N., Akamatsu, K., et al. (2019). Predictive value of serum protein levels in patients with advanced non-small cell lung cancer treated with nivolumab. Lung Cancer *132*, 107–113.
42. Deng, B., Yang, B., Chen, J., Wang, S., Zhang, W., Guo, Y., Han, Y., Li, H., Dang, Y., Yuan, Y., et al. (2022). Gallic acid induces T-helper-1-like T(reg) cells and strengthens immune checkpoint blockade efficacy. J. Immunother. Cancer *10*, e004037.
43. Sullivan, R.J., and Weber, J.S. (2022). Immune-related toxicities of checkpoint inhibitors: mechanisms and mitigation strategies. Nat. Rev. Drug Discov. *21*, 495–508.
44. Zhu, H., Galdos, F.X., Lee, D., Waliany, S., Huang, Y.V., Ryan, J., Dang, K., Neal, J.W., Wakelee, H.A., Reddy, S.A., et al. (2022). Identification of Pathogenic Immune Cell Subsets Associated With Checkpoint Inhibitor-Induced Myocarditis. Circulation *146*, 316–335.
45. Liu, X., Hartman, C.L., Li, L., Albert, C.J., Si, F., Gao, A., Huang, L., Zhao, Y., Lin, W., Hsueh, E.C., et al. (2021). Reprogramming lipid metabolism prevents effector T cell

senescence and enhances tumor immunotherapy. Sci. Transl. Med. *13*, eaaz6314.

46. Lioulios, G., Fylaktou, A., Papagianni, A., and Stangou, M. (2021). T cell markers recount the course of immunosenescence in healthy individuals and chronic kidney disease. Clin. Immunol. *225*, 108685.
47. Ron-Harel, N., Notarangelo, G., Ghergurovich, J.M., Paulo, J.A., Sage, P.T., Santos, D., Satterstrom, F.K., Gygi, S.P., Rabinowitz, J.D., Sharpe, A.H., and Haigis, M.C. (2018). Defective respiration and one-carbon metabolism contribute to impaired naïve T cell activation in aged mice. Proc. Natl. Acad. Sci. USA *115*, 13347–13352.
48. Ma, J., Chen, T., Wu, S., Yang, C., Bai, M., Shu, K., Li, K., Zhang, G., Jin, Z., He, F., et al. (2019). iProX: an integrated proteome resource. Nucleic Acids Res. *47*, D1211–D1217.
49. Chen, T., Ma, J., Liu, Y., Chen, Z., Xiao, N., Lu, Y., Fu, Y., Yang, C., Li, M., Wu, S., et al. (2022). iProX in 2021: connecting proteomics data sharing with big data. Nucleic Acids Res. *50*, D1522–D1527.
50. Yurekten, O., Payne, T., Tejera, N., Amaladoss, F.X., Martin, C., Williams, M., and O'Donovan, C. (2024). MetaboLights: open data repository for metabolomics. Nucleic Acids Res. *52*, D640–D646.
51. Baggerly, K.A., Morris, J.S., Edmonson, S.R., and Coombes, K.R. (2005). Signal in noise: evaluating reported reproducibility of serum proteomic tests for ovarian cancer. J. Natl. Cancer Inst. *97*, 307–309.

STAR★METHODS

KEY RESOURCES TABLE

REAGENT or RESOURCE	SOURCE	IDENTIFIER
Antibodies		
Anti-Human CD45	BD Bioscience	Cat#347463; RRID:AB_400306
Anti-Human CD3	BD Bioscience	Cat#555332; RRID:AB_395739
Anti-Human CD4	BD Bioscience	Cat#566320; RRID:AB_2739682
Anti-Human CD8	BD Bioscience	Cat#561948; RRID:AB_11154582
Anti-Human CD16	BD Bioscience	Cat#556618; RRID:AB_396490
Anti-Human CD56	BD Bioscience	Cat#562794; RRID:AB_2737799
Anti-Human CD19	BD Bioscience	Cat#555412; RRID:AB_395812
Anti-Human CD28	BD Bioscience	Cat#556621; RRID:AB_396493
Biological samples		
Peripheral blood samples	This study	N/A
Chemicals, peptides, and recombinant proteins		
SDS	Sigma	Cat#75746-250G
Tris-HCl	Bio-rad	Cat#1610719
Trypsin	Beijing Hualishi Technology Co.	Cat#HLS TRY001C
Formylic acid	Shanghai Titan Technology Co.	Cat#F0654-25mL
Acetonitrile	Fisher scientific	Cat#A955-4-CASE
Methanol	Fisher chemical	Cat#A456-4
Ammonia	Fisher chemical	Cat#A470-500
Ammonium acetate	Sigma	Cat#73594
Nuclease-free water	ThermoFisher	Cat#10977015/10977-023
Zeba™ Spin Desalting Columns, 7K MWCO，0.5mL	ThermoFisher	Cat#89883
ACQUITY UPLC BEH Amide 1.7 μm, 2.1 mm × 100 mm column	WATERS	Cat#186002352
Critical commercial assays		
ProcartaPlex Human Cytokine/Chemokine/ Growth Factor Panel 1 (45 plex)	ThermoFisher	Cat#EPX450-12171-901
Immuno-Oncology Checkpoint 14-PL ex ProcartaPlex Panel	ThermoFisher	Cat#EPX14A-15803-901
Pierce™ High pH Reversed-Phase Peptide Fractionation Kit	ThermoFisher	Cat#84868
Deposited data		
Processed data	This study	https://doi.org/10.5281/zenodo.10871944
Raw data for proteomics data	This study	iProX: IPX0008520000[48,49]
Raw data for metabolomics data	This study	MetaboLights: MTBLS9977[50]
Software and algorithms		
Spectronaut software	N/A	Spectronaut™ 14.4.200727.47784
FACSDiva Software	BD Bioscience	https://www.bdbiosciences.com/
R software (v. 3.6.3)	R project	https://www.r-project.org/
GraphPad PRISM 8.0	GraphPad Software	https://www.graphpad.com/scientific-software/prism/

RESOURCE AVAILABILITY

Lead contact

Further information and requests should be directed and will be fulfilled by the lead contact, Lin Li (lilin_51@hotmail.com).

Materials availability

This study did not generate new unique reagents.

Data and code availability

- Data generated in this study have been deposited at MetaboLights and iProX. Processed data have been deposited at Zenodo. Accession numbers and DOIs are listed in the key resources table. Any additional information required to reanalyze the data reported in this paper is available via request from lead contact, Lin Li (lilin_51@hotmail.com).
- This paper does not report original code.
- This paper does not contain any other item.

EXPERIMENTAL MODEL AND STUDY PARTICIPANT DETAILS

The expedient model in this work was limited to human subjects. The average age of the patients was 70 years old, 76% were males and 24% were females. All patients were Chinese. All the patients were diagnosed with NSCLC and were treated with immune checkpoint inhibits in our institute. The study was conducted in accordance with the Declaration of Helsinki, and approved by the ethics committee of Beijing Hospital, National Center of Gerontology; Institute of Geriatric Medicine, Chinese Academy of Medical Sciences (Beijing, China; approved 2023BJYYEC-028-02).

METHOD DETAILS

Study design and populations

Patients aged ≥65 years with unresectable stage III-IV NSCLC who were first treated with anti-PD-1 antibodies, either as monotherapy or in combination with chemotherapy at Beijing hospital were enrolled in this study from July 2019 and March 2022. All patients provided written informed consent for the research approved by the ethics committee of Beijing Hospital, National Center of Gerontology; Institute of Geriatric Medicine, Chinese Academy of Medical Sciences. Patients with either alteration in EGFR, ALK and ROS1 were excluded. There was no history of autoimmune phenomena, allergic conditions or current steroid use in our cohort. All patients were followed until the deadline of December 31, 2022 or the death of the patient. Potential immune-related adverse effects were evaluated by at least 2 medical professionals and graded according to the Common Terminology Criteria Adverse Events V5.0. Clinical response was evaluated by the Response Evaluation Criteria in Solid Tumors V1.1, including complete response (CR), partial response (PR), stable disease (SD), and progressive disease (PD). Each patient received at least one efficacy evaluation. For the efficiency analysis, patients were defined as responders based on at least one evaluation of PR or CR, while non-responders were patients who did not achieve PR or CR up to the last treatment.

Sample collection and preparation

Blood samples taken at fasting at three time points (pre-treatment, after 1–2 cycles and the onset of irAEs) were collected into 5 mL- EDTA whole blood tubes. Each patient was required to fast for at least 6 h before blood sample collection. Samples were centrifuged for 10 min (1500g, 4°C) no later than 4 h after blood sample collection. Each aliquot (300 μL) of the plasma sample was stored at −80°C for storage.

Plasma multiplex immunoassay

Plasma samples were analyzed with a 45-plex ProcartaPlex Human Cytokine/Chemokine/Growth Factor Panel (Affymetrix, Inc.) and 14-plex ProcartaPlex Human Immuno-Oncology Checkpoint Panel (Affymetrix, Inc.). The antigen standard was gradient diluted according to the specification. Add 50μL magnetic beads to each reaction well and wash twice with wash buffer. Magnetic beads containing antibody were incubated with samples or standards substance at 4° C for 16 h, then 25 μL of detection antibody was added and mixed at room temperature for 30 min. The antigen-antibody binding was detected by Luminex MAGPIX instrument (Thermo Scientific, USA) according to its instructions. Data analysis was performed using ProcartaPlex Analyst 1.0 software. Cytokine concentration (pg/mL) were measured by fitting a standard curve for average fluorescence intensity versus concentration.

Flow cytometry

Peripheral blood lymphocyte subsets analysis was performed by flow cytometry. Fresh blood was collected in 5mL- EDTA whole blood tubes prior to initial ICI infusion. For surface marker detection, cells were stained with anti-CD45, anti-CD3, anti-CD4, anti-CD8, anti-CD16, anti-CD56, anti-CD19 and anti-CD28 (BD Biosciences). After samples were incubated for 20 min at room temperature protected from light, red cells were lysed using red blood cell lysis buffer. Cells were then acquired using the BD FACSCanto II, and data were analyzed using BD FACSDiva Software.

Protein extraction and peptide enzymolysis

Analysis was performed in Shanghai Applied Protein Technology Co., Ltd. Appropriate amount of SDT (4%SDS, 100mM Tris-HCl, pH7.6) lysate was added to each sample for protein extraction. Protein concentration was quantified with the standard BCA method. The amount of 20μg protein was taken from each sample and added into an appropriate amount of 5X loading buffer for SDS-PAGE electrophoresis. Appropriate amount of protein was obtained from all samples and mixed into pool samples to establish a Spectral Library. All samples, including mixed pool samples, were enzymolysis by Filter aided proteome preparation (FASP). Appropriate amount of iRT standard peptide was added to pool sample peptide and enzymolysis peptide of each sample for DDA mass spectrometry and DIA mass spectrometry detection.

LC-MS/MS analysis

For proteomics analysis, DDA analysis was performed by Easy-nLC 1200 HPLC system with sodium-litre flow rate. The samples were injected into a C18 column (Thermo Scientific, ES802, 1.9 μm, 75 μm*20 cm) for linear gradient separation (0.1% acetonitrile solution (84% acetonitrile) at a flow rate of 300 nL/min). Samples were then performed using Q-exactive HF-X mass spectrometer (Thermo Scientific, USA). Detection mode: positive ion. Primary mass spectrum scanning range: 350–1800 m/z, mass spectrum resolution: 60,000 (@m/z 200), AGC target: 1e5, Maximum IT: 50 ms, dynamic exclusion time: 10s. After each full MS scan, 20 ddMS2 scans are collected according to the inclusion list. Isolation window: 1.5m/z, mass spectrum resolution: 30,000 (@m/z 200), AGC target: 1e5, Maximum IT: 50 ms, MS2 Activation Type: HCD, Normalized collision energy: 30 eV. DIA analysis was performed by Easy-nLC 1200 HPLC system with sodium-litre flow rate. Samples were then performed using Q-exactive HF-X mass spectrometer. Detection mode: positive ion. Primary mass spectrum scanning range: 350–1800 m/z, mass spectrum resolution: 120,000 (@m/z 200), AGC target: 3e6, Maximum IT: 30 ms. MS2 adopts DIA data acquisition mode and sets 44 DIA acquisition Windows. Mass spectrum resolution: 30,000 (@m/z 200), AGC target: 3e6, Maximum IT: 30 ms, Maximum IT: auto, MS2 Activation Type: HCD , Normalized collision energy: 30 eV, Spectral data type: profile.

For metabolomics analysis, analysis was performed using an UHPLC (1290 Infinity LC, Agilent Technologies) coupled to a quadrupole time-of-flight (AB Sciex TripleTOF 6600) in Shanghai Applied Protein Technology Co., Ltd. For HILIC separation, samples were analyzed using a 2.1 mm × 100 mm ACQUIY UPLC BEH Amide 1.7 μm column (waters, Ireland). In both ESI positive and negative modes, the mobile phase contained A = 25 mM ammonium acetate and 25 mM ammonium hydroxide in water and B = acetonitrile. The gradient was 95% B for 0.5 min and was linearly reduced to 65% in 6.5 min, and then was reduced to 40% in 1 min and kept for 1 min, and then increased to 95% in 0.1 min, with a 3 min re-equilibration period employed. The ESI source conditions were set as follows: Ion Source Gas1 (Gas1) as 60, Ion Source Gas2 (Gas2) as 60, curtain gas (CUR) as 30, source temperature: 600°C, IonSpray Voltage Floating (ISVF) ± 5500 V. In MS only acquisition, the instrument was set to acquire over the m/z range 60–1000 Da, and the accumulation time for TOF MS scan was set at 0.20 s/spectra. In auto MS/MS acquisition, the instrument was set to acquire over the m/z range 25–1000 Da, and the accumulation time for product ion scan was set at 0.05 s/spectra. The product ion scan is acquired using information dependent acquisition (IDA) with high sensitivity mode selected. The parameters were set as follows: the collision energy (CE) was fixed at 35 V with ±15 eV; declustering potential (DP), 60 V (+) and −60 V (−); exclude isotopes within 4 Da, candidate ions to monitor per cycle: 10.

Quality control evaluation

In order to monitor and evaluate the stability of the system and the reliability of the experimental data, a quality control (QC) sample (a mixed sample of all samples) was inserted into the sample queue at an interval of a certain number of samples. For proteomics analysis, coefficient of variation (CV), pearson correlation analysis were used to evaluate the quality of QC samples. Column peak capacity statistics in DIA test, distribution of protein FDR and elution time for each peptide of iRT Kit on the chromatogram were all demonstrated a stable DIA system.

For metabolomics analysis, Total ion chromatogram (TIC), Hotelling's T2 test, multivariate control chart and relative standard deviation (RSD) were used to evaluate the quality of QC samples. (Figures S7 and S8)

Data analysis

DDA data was directly imported to Spectronaut software (SpectronautTM14.4.200727.47784) build a Spectral Library. Download the database according to the species. Search parameters were set as follows: the enzyme as trypsin, the max miss cleavage site as 1, the fixed modification as Carbamidomethyl (C), and the dynamic modification as Oxidation (M) and Acetyl (Protein N-term). The protein identified by database search must pass the set filtering parameter FDR<1%. DIA data was processed using Spectronaut software (SpectronautTM 14.4.200727.47784) and the database was the same as that used for the construction of the database. Software parameters were set as follows: retention time prediction type as dynamic iRT, interference on MS2 level as enabled, cross run normalization as enabled. All results must pass the filter parameter Q Value cutoff of 0.01 (equivalent to FDR<1%).

The raw MS data were converted to MzXML files using ProteoWizard MSConvert before importing into freely available XCMS software. For peak picking, the following parameters were used: centWave m/z = 10 ppm, peakwidth = c (10, 60), prefilter = c (10, 100). For peak grouping, bw = 5, mzwid = 0.025, minfrac = 0.5 were used. CAMERA (Collection of Algorithms of MEtabolite pRofile Annotation) was sued for annotation of isotopes and adducts. In the extracted ion features, only the variables having more than 50% of the nonzero measurement values in at least one group were kept. Compound identification of metabolites was performed by comparing of accuracy m/z value.

Bioinformatic analysis

The functional enrichment analysis Gene Ontology (GO) and Kyoto Encyclopedia of Genes and Genomes (KEGG) was applied by the GO and KEGG library. The significance level of the enrichment pathway was analyzed by Fisher's exact test. The trend of protein expression over time was analyzed by fuzzy c-means algorithm (FCM). The above were analyzed and graphed using R software V.3.6.3.

Ensemble learning method

The ensemble learning method[51] was designed to select biomarkers. It integrates multiple types of machine learning algorithms to identify potential targets that frequently appear in classification models with high accuracy. The reward scores obtained in five feature selection methods (logistic regression (LR), support vector machine (SVM), Boruta based on random forest (RF), recursive feature elimination, and correlation-based feature selection were calculated as a comprehensive weight value for each substance. All substances were sorted from high to low according to their weight. Receiver operating characteristic (ROC) accumulating curves were calculated by fitting LR and linear models to further identify the biomarkers. Finally, we trained a logistic regression model using screened biomarkers to identify older patients with higher risk of irAEs.

QUANTIFICATION AND STATISTICAL ANALYSIS

Statistical analyses were performed using R software V.3.6.3 and SPSS V.23. For both proteomics and metabolomics data, a t-test was performed on the scaled imputed data to determine the significance of the differences. Differentially expressed proteins were then screened using a cut-off of p value <0.05, fold change >1.5 or fold change <0.67. For metabolomics data, the variable importance in the projection (VIP) was calculated by orthogonal partial least-squares discriminant analysis (OPLS-DA). Permutation test and 7-fold cross-validation verified the reliability of the model. Differentially changed metabolites were screened using a cut-off of p value <0.05 and VIP >1. For comparisons of more than two groups, one-way ANOVA was employed for normal distributions and homogeneity of variance, and the Kruskal–Wallis test for non-normal or inhomogeneity of variance. Bonferroni adjustment was used for pairwise comparisons. Chi-square test or Fisher exact tests were used for rate comparison. Kaplan–Meier method was used to calculated progression-free survival (PFS) curves and log-rank test was used to seek for differences between the two groups. Univariate and multivariable survival analyses were estimated by the Cox proportional hazards model. A two-sided α of <0.05 was considered to indicate statistical significance.